Personalized Dosimetry for ^{188}Re Radionuclide Therapies Based on Post-Treatment SPECT/CT Scans

Anna Celler[1,*] and Pedro L. Esquinas[2]

[1]*Department of Radiology, University of British Columbia, Vancouver, BC, V5Z 1M9, Canada*

[2]*Department of Physics and Astronomy, University of British Columbia, Vancouver, BC, V6T 1Z1, Canada*

Abstract: Over the last three decades, Rhenium-188 (^{188}Re) applications in Nuclear Medicine therapies have gathered a lot of interest thanks to the favorable physical and chemical characteristics of this isotope. In order to optimize ^{188}Re therapies, the accurate knowledge of the activity distribution within the patient body is required. To this end, the nuclear medicine images must yield accurate quantitative measurements. However, the decay of ^{188}Re results in a large variety of emissions such as β-particles, γ-particles and Bremsstrahlung, making quantitative measurements of ^{188}Re activity a very difficult task. In this paper, we discuss the imaging protocols, data acquisitions, techniques used in image reconstruction and processing, and dose estimation methods required for accurate, image-based, personalized dosimetry for molecular therapies with ^{188}Re.

Keywords: Rhenium-188, Radionuclide therapies, Quantitative SPECT, Image segmentation, dosimetry

1. INTRODUCTION

The use of radioisotopes in cancer therapies has already a long history, dating from early 1900s when first experimental treatments of skin diseases with radium-226 (^{226}Ra) were performed [1, 2]. Later, therapies with iodine-131 (^{131}I), phosphorous-32 (^{32}P), strontium-90 (^{90}Sr), and yttrium-90 (^{90}Y) have been developed and successfully used for treatment of thyroid nodules and many other malignant and benign conditions. However, only recently increased awareness of the need for treatment strategies which will be tailored for individual patient's needs (personalized medicine) has led to a tremendous growth in targeted radionuclide therapies, with many new pharmaceuticals and new radioisotopes being tested in clinical trial and being introduced into practice [3-5].

The principle of targeted radionuclide therapy (TRT) relies on the use of a molecular carrier, labeled with a radioisotope, to deliver high radiation dose directly to the tumour. Typically, radioisotopes which are used in TRT decay with the emission of high energy massive particles (electrons or alphas), in contrast to electromagnetic radiation predominantly used in external beam radiotherapy (EBRT). These particles will deposit all their energy in the close proximity of the area with high radiopharmaceutical uptake, sparing areas with low uptake. For this reason, the search for molecules which will selectively concentrate and remain in the tumor cells, thus allowing for a very localized dose delivery, is extremely important. Another critical issue is the development of methods to estimate delivered doses.

Nuclear medicine (NM) imaging studies (SPECT and PET), performed before treatment (using molecules labeled with diagnostic radioisotopes, such as ^{99m}Tc, ^{111}In, ^{68}Ga or others) and/or after treatment (using molecules labeled with therapeutic radioisotope), provide information about radiopharmaceutical distribution in the patient body. This information can be used for the initial diagnosis of the disease and, after the treatment, for confirmation of the delivered therapy. Additionally, they can be used for the personalized, image-based dosimetry calculations, which are necessary to estimate the dose delivered to tumour(s), and also to healthy tissues, most importantly, to organs at risk.

Since large inter-patient variability observed in radiotracer uptakes [6-8] may potentially lead to dangerous consequences, personalized dosimetry calculations should be performed for every patient to optimize his/her therapy outcomes and to minimize toxicity. For calculation of absorbed radiation doses quantitative information about the distribution of the radioactive material in the patient body and accurate information about changes in this activity distribution are required. These two pieces of information can be relatively easily obtained if the therapy radioisotope, besides electrons or alphas which are used to kill tumour cells, emits also gamma radiation which could be used for imaging. Several isotopes fulfill this

*Address correspondence to this author at the Department of Radiology, University of British Columbia, Vancouver, BC, V5Z 1M9, Canada;
Tel: (+1) 604 875-5252;
E-mail: aceller@physics.ubc.ca

E-ISSN: 2408-9788/17

Table 1: Characteristics of the ^{188}Re Emissions (Only Emissions having Yields >1% are Listed) [51]

^{188}Re	$T_{1/2}$	β^-		γ	
		E_{max} (keV)	I (%)	E (keV)	I (%)
	17 hours	1487.4	1.75	61-63 (X-rays)	3.8
		1965.4	26.3	71-73 (X-rays)	1.01
		2120.4	70.0	155.04	15.61
				477.99	1.08
				632.98	1.37

condition (for example, see Table **1** in MIRD Pamphlet 23 [9]) and ^{188}Re is one of them.

In this paper, we provide a general review of the techniques used in personalized dosimetry calculation for radionuclide therapy patients. The key elements of the procedures, including imaging protocols, data acquisition, image reconstruction and processing, and dose estimation methods are discussed. The second part of the paper focuses on dosimetry for patients undergoing radionuclide therapies with ^{188}Re. The challenges which are encountered when performing patient-specific dosimetry for this radioisotope are analyzed using examples of phantom and patient studies.

2. PERSONALIZED DOSIMETRY FOR RADIO-NUCLIDE THERAPY

In theory, radionuclide therapy should follow the same protocol as is used in EBRT. In EBRT, a treatment plan is created for each patient, based on personalized dosimetry calculations, aiming to deliver high radiation dose to the tumour(s), while maintaining radiation dose to organs at risk (OAR) below threshold levels to minimize adverse effects. Unfortunately, this is not a routine approach in radionuclide therapies; here typically empirically determined or fixed activities are being administered to all patients. Often patient weight, evaluation of lung shunt and ratio of tumour volume to normal liver are the only factors considered when calculating radiopharmaceutical activity to be administered [10-12].

Personalized dosimetry calculations for radionuclide therapies are not routinely done because they are considered to be difficult, time consuming and expensive. However, there are data suggesting that TRT efficacy could be substantially improved by therapy personalization [13]. Fortunately, recent studies [6, 14, 15] have shown that personalized dosimetry calculations are possible when using a quantitative image reconstruction, advanced image analysis and dose calculation algorithms. The use of these techniques is also recommended by the recent MIRD pamphlet 23 [9] as only when using them the most appropriate activity to be administered to each individual patient can be determined.

2.1. Internal Dosimetry Calculations

Dosimetry calculations for internally administered radioisotopes are normally based on the data derived from scintigraphic scans (planar and/or single photon emission computed tomography – SPECT) or positron emission tomography (PET) imaging studies that can be combined with data from blood and/or urine sampling. The absorbed radiation dose delivered to an organ is equal to the energy deposited by all types of emitted radiation in this organ. It depends on the fraction of administered activity that accumulates and is subsequently retained in or cleared from this organ, as well as the accumulation and clearance from surrounding tissues. This fraction depends on the radiopharmaceutical kinetics and tissue properties, both of which are subject to patient-specific factors causing mentioned above inter-patient variability of the absorbed radiation dose per unit of administered activity.

To summarize, the personalized TRT dosimetry has to take into account both patient-related variables and physics-related factors. There are two main patient-related challenges in internal dosimetry: (1) to accurately determine the distribution of the injected radiopharmaceutical in different tissues and (2) to determine the pharmacokinetics of the agent in question in each tissue of interest. As already mentioned, these must be obtained from the imaging scans of a particular patient. Based on this information,

the amount of deposited energy (dose) and the distribution of this deposited energy (dose map) can be determined. Physics related factors are the types (particles or gammas) and the energies of radioactive emissions and the densities of tissues. Additionally, absorbed dose in tumours, OARs and other organs will depend on the distances between tumours and organs with high uptake (they will contribute to dose estimate in their neighborhood) and OARs and other sensitive organs.

These dependencies can be expressed in a mathematical form. According to MIRD schema [16] the mean dose $D(r_T, T_D)$, absorbed in the target tissue, r_T, over the dose-integration period, T_D, can be calculated using the following equation:

$$D(r_T, T_D) = \sum_{r_S} \widetilde{A}(r_S, T_D) S(r_T \leftarrow r_S),$$

where: $\tilde{A}(r_S, T_D)$ corresponds to the time-integrated activity in source organ r_S over T_D, and the factor $S(r_T \leftarrow r_S)$ represents the dose absorbed in r_T per one decay of the radioisotope contained in r_S.

Dosimetry calculations can be performed using the "organ-level" approach, which assumes an average organ shape and mass and activity that is uniformly distributed throughout that organ. Organ-level calculations determine an average dose in the entire organ. Alternatively, "voxel-level" calculations can be performed allowing the user to create 3-dimensional (3D) maps of dose distribution within the organ or the entire body.

Organ-level dosimetry calculations rely on the tabulated values of the S-factors [17, 18]. These S-factors combine the physics-related information about the energies deposited by the radioactive emissions and are radioisotope-specific, with the geometrical information about the relative positions of organs in the body. Unfortunately, the tabulated S-factors have been created using Monte Carlo (MC) simulations of model human subjects which usually only very roughly approximate any particular patient anatomy [19, 20].

Alternatively, for voxel-level calculations, the maps of activity distribution can be convolved with maps describing energy deposition by a given radioisotope in soft tissue (voxelized S-values). Although this type of calculation takes into account characteristics of the radiotracer uptake of the individual patient and his/her anatomy, still it assumes uniform distribution of tissue densities [21]. The voxelized S-values have been tabulated for many radiotherapy isotopes and several voxel sizes and are freely available [22].

The most accurate, but also the most difficult to perform and time consuming dosimetry calculation will use the 3D images of activity distribution (from NM studies) and images of tissue density (from CT studies) to perform full MC simulation of the particle transport in the patient body. In this calculation each particle emitted by the radioisotope will be followed as it travels through different types of tissue and deposits its energy [23, 24].

As mentioned, the advantage of both the Voxelized S-Value method and the full MC simulation is that both these methods allow us to obtain 3-D maps of the dose distribution which subsequently can be segmented to provide dose values equivalent to those obtained from organ-level calculations, or can be used to generate dose-volume histograms, commonly used in EBRT.

2.2. Quantification of Activity

Conventional dosimetry calculations have almost always been based on planar imaging, the accuracy of which is limited by organ/tumour superimposition and background activity [25, 26]. Additionally, attenuation correction for planar images is only very approximate as, at best, it can use transmission maps measured using an uncollimated flood source. On the other hand, SPECT, a 3D imaging technique, overcomes these limitations and hybrid SPECT cameras combined with X-ray computed tomography (SPECT/CT) routinely compensate for attenuation. Also, in order to obtain truly quantitative results, corrections for other effects (*e.g.*, scatter, dead-time and resolution loss) must be implemented [9]. Additionally, to determine pharmacokinetics (uptake and washout) of the radiotracer, a series of imaging scans must be performed over the time when activity changes are expected to occur.

Iterative reconstruction methods, such as, maximum likelihood expectation maximization [27] or ordered subsets expectation maximization (OSEM) [28], are required for quantitative reconstruction because they allow for optimal implementation of corrections. As modern SPECT cameras are typically combined with CT scanners, attenuation correction (AC) uses patient-specific attenuation maps obtained from the CT images. Additionally, accurate quantification of images requires scatter correction (SC) to be performed.

Several techniques have been proposed for scatter correction [29]. They range from relatively complex MC simulation-based approaches, through analytical scatter calculation to the simplest re-scaling of the attenuation map to the broad-beam coefficient values. However, this last method corrects only the total number of counts, not photon distribution. One of the simpler and also probably the most popular method is the triple energy window (TEW) technique [30] which corrects for the scattered photopeak photons (self-scatter) and also can account for contributions from the scattered high energy photons and the background. The TEW method generates only an approximate estimate of scattered photon distribution, but the effect of this approximation is very unlikely to affect accuracy of patient studies.

Finally, correction for collimator-detector response (CDR) is often included in the reconstruction. Although this correction does not change the total number of counts in the reconstructed image (so it does not affect quantitative accuracy), it improves image resolution thus decreases partial volume effect. The attenuation correction and the correction for the collimator-detector response (CDR) are usually incorporated directly into the system matrix of the reconstruction algorithm, while scatter correction is included only in the projector part of the algorithm.

One more source of potential errors in activity quantification for radionuclide therapies is related to the detector dead-time observed when high levels of activity are administered. In most therapeutic studies, the correction for the dead-time is necessary only for the first imaging time-point as it is then when a very large flux of photons strikes the detector. The lack of dead-time corrections would cause under-estimation of activities in tumors and OARs. As a result, the pharmacokinetic information would not be accurately determined, affecting the accuracy of the dosimetry estimates.

There are two methods to determine dead-time correction factors (DTCFs) which can be used in this case. In the first approach, the DTCFs are determined using phantom calibration experiments [31, 32]. In the second method, a marker (point-source) of well-known activity is placed within the scanner field-of-view and its count-rates are measured with and without the patient in place. The DTCF is determined from the ratio of counts in a small region of interest (ROI) drawn around the marker in the patient + marker scan (where the dead-time is present) and the marker alone scan [33].

Finally, in order to convert the counts in the reconstructed image into the units of activity (or activity concentration), a system calibration factor must be applied. The system calibration factor, k, can be determined by acquiring a tomographic acquisition of an extended phantom filled with activity or using a planar image of a point-source. In both cases the activity of the isotope of interest must be accurately known prior to the scan, and k is obtained using the following formula [34, 35]:

$$k = \frac{C}{t \times A}$$

Where: C represents the total reconstructed counts in the phantom image, or in the case of planar scan, the image counts recorded in the photopeak window; t represents the acquisition time of the scan and A represents the activity of the isotope. During the acquisition, the energy window settings must be identical to those selected for the patient SPECT scans. The point-source calibration method relies on the assumption that scatter and attenuation within the point-source are minimal, so the measured counts in the photopeak window represent the primary photons only. If the isotope's emissions include high-energy photons which may scatter into photopeak window (like is the case in ^{188}Re), the TEW method should be applied to remove them from the photopeak window.

2.3. The Imaging Protocols

As discussed in Section 2.1, in order to evaluate the dose absorbed in an ROI (organ or tumour), the activity distribution in the tissue must be quantified, as well as temporal changes of this activity distribution (pharmacokinetics) must be determined. This last step requires collecting imaging data at multiple time-points (typically at least 2-3) and creating time-activity-curves (TACs) for every source region or organ, or even for every voxel in the image. The data necessary for TACs creation can be acquired using three different approaches:

1. Planar scans only - the TACs are generated using a series of planar scans (often whole body - WB) where only approximate quantification of activity is performed.

2. Hybrid method – the TACs are generated as in the planar-only method. Next, TACs are renormalized using a single quantitative SPECT image acquired during the time period covered

by the TAC and performed over the area which includes all organs and regions of interest.

3. SPECT scans only – the TACs are generated using data from a series of fully quantitative 3D images. The use of SPECT/CT for accurate 3D dosimetry calculations has been recommended by one of the latest MIRD (Medical Internal Radiation Dose) publications [9].

In order to create TACs, all the images in the series that will be used for TACs creation must be co-registered to each other and the counts in the organs or regions of interest (source regions) at different time points summed. The acquired data can then be plotted versus time to form TACs corresponding to all source regions. By fitting mono or even multi-exponential curves to these data and integrating the areas under the curve, the values of $\tilde{A}(r_S)$ for each source region can be calculated. In order to determine the exact value of the time integrated activity, it is important to collect the data over a sufficiently long time interval (usually should be longer or much longer than the physical half-life of the isotope).

Co-registration of images obtained from a sequence of scans may be quite challenging, as patient position often changes during different imaging sessions, and also activity distribution changes over time. For planar images, co-registration often uses rigid transformation and attempts to match organ boundaries. Then, organs and tumours of interest must be segmented and TACs are created for them, assuming pharmacokinetics to be the same in all voxels of each region. When a series of SPECT/CT scans is performed, 3D co-registration and 3D segmentation are required. In principle, such co-registration can be done using CT images from each scan, however, it is still difficult and there is no guarantee that SPECT and CT images (which are always acquired sequentially) are perfectly matched. In theory, co-registered 3D SPECT images can be used to generate TACs for every voxel. Such TACs, however, not only are extremely noisy, but also there is no guarantee that voxel matching was done correctly and that the registration process did not change the distribution of activity. Therefore, even in this case it is safe to assume the same pharmacokinetics in all voxels of each organ, similar to planar scans.

2.4. Organ Segmentation

Another, very challenging problem is segmentation of organs and tumours in NM images. The problem is difficult, due to poor resolution of these images (partial volume effect) and often non-negligible spill-in and spill-out between different regions. Nevertheless, such segmentation is necessary for generation of TACs, where activity in the source organs must be estimated in a series of images. Additionally, segmentation must be performed for calculation of mean doses absorbed in different target organs and regions. This can be done by segmenting quantitative images of activity distribution prior to performing organ-based dosimetry to obtain organ mean doses. Alternatively, images of activity distribution may be convolved with voxelized matrices of energy deposition to create dosimetry maps, which can also be segmented to calculate mean doses in the segmented regions.

The most obvious segmentation method would be to manually draw ROI boundaries. This approach is relatively straightforward when segmenting planar images, but very tedious and difficult when a series of ROI must be drawn in 3D. Additionally, this segmentation is very subjective and may depend on the colour-scale used to display the image. Other methods which are quite popular in clinical studies, is to use organ boundaries visible in CT images or to create ROIs using a fixed threshold, and threshold values between 40-50% have been used [36, 37]. Due to the partial volume effect, CT-based segmentation always underestimates activity in the hot regions (and underestimates in cold areas), while fixed threshold method may produce variable results, highly dependent on the distribution of activity in the organ of interest and its immediate neighbourhood. Many more segmentation methods with variable complexity have been studied [38]. In particular, adaptive thresholds have been proposed, where the threshold value varies depending on the signal-to-background (SBR) ratio [39]. A modification of this method proposes to use two thresholds: one for segmentation of activity, another for organ volume. The curves showing these thresholds dependency on the SBR must be determined using phantom experiments [40].

Accurate segmentation of NM images (both SPECT and PET) is certainly a very important problem, which is currently actively investigated by many researchers [41].

3. DOSIMETRY FOR ^{188}Re RADIONUCLIDE THERAPIES

3.1. Current Radiotherapies with ^{188}Re

Currently, there are numerous clinical applications of ^{188}Re radiolabeled pharmaceuticals in radionuclide

therapies [10]. They range from palliative treatment of painful bone metastases from breast [42] and prostate cancer [43] using ^{188}Re-HEDP, radiation synovectomy treatments with^{188}Re-colloids [44, 45], endovascular brachytherapy using liquid ^{188}Re-perrhenate for patients with in-stent stenosis [46], radioimmuno-therapy applications using ^{188}Re-labelled monoclonal antibodies [47, 48], to targeted therapy for lung cancers using ^{188}Re-labelled somatostatin analogs [49] and trans-arterial radioembolization (TARE) therapy for liver cancers using ^{188}Re-HDD Lipiodol [11, 50] and ^{188}Re-Human Serum Albumin (HSA) [12, 51].

The largest clinical experience using ^{188}Re-HDD Lipiodol as a radioembolization agent comes from a study sponsored by the International Atomic Energy Agency (IAEA) which involved centers from 8 countries and 185 patients [11, 50]. The IAEA study aimed to tailor the therapy for each patient by performing, prior to the treatment, a whole-body planar scan using a low ('scout') activity of ^{188}Re-HDD Lipiodol (~200 MBq). From this scan, the maximum tolerated activity was determined by estimating the radiation absorbed dose to critical organs [55]. Based on previous pharmacokinetics studies of ^{131}I-HDD-Lipiodol [53], the clearance of ^{188}Re-HDD-Lipiodol in tissue (tumour, liver and lungs) was assumed to follow a mono-exponential function with effective half-life of 17h (*i.e*., equal to ^{188}Re physical half-life). However, this assumption was not verified during treatment due to the lack of post-therapy imaging.

The clinical experience with ^{188}Re-HSA radioembolization involves two small patient studies done in Europe [12, 51]. Liepe *et al.* 2007 [51] investigated the feasibility of high-activity ^{188}Re-HSA radioembolization. In this work, the pharmacokinetics of ^{188}Re-HSA were determined based on post-therapeutic whole-body scans acquired at 24h, 48h, 72h and 96h post-treatment. Despite the embolic properties of HSA, the authors measured the effective half-life of ^{188}Re-HSA in tumor to be approximately 16h, which is slightly less than the physical half-life of ^{188}Re. The difference was explained by the biological washout of the free ^{188}Re that was present in the injected radiopharmaceutical. The uptake in the liver and liver metastases was measured using a single SPECT image acquired 48h post-therapy using a window centered at the 155keV photopeak of ^{188}Re. However, this measurement might not be quantitatively accurate as SPECT image was not corrected for scatter.

As will be shown in Sections 3.4 and 3.5, the accuracy of dosimetry estimates strongly depends on the accuracy of activity quantification and also on the accurate knowledge of its change over time (effective half-life). However, in our opinion, the effective half-life of ^{188}Re in some of the radioembolization studies discussed above was not rigorously determined. The study performed by Nowicki *et al* 2014 [12] utilized quantitatively accurate ^{188}Re SPECT images for patient-specific dosimetry of ^{188}Re-HSA [34]. In this study, dosimetry was estimated using ^{188}Re physical decay half-life as it was assumed that the microspheres remained in the liver permanently. However, this assumption was never verified.

The determination of the effective half-life of ^{188}Re-Lipidol was modeled based on the study with Lipidol labeled with ^{131}I, which might not have the same pharmacokinetics as ^{188}Re. The investigation of ^{188}Re-HDD Lipiodol pharmacokinetics is especially important because Lipiodol does not behave like a physical embolic agent (as compared to glass or resin microspheres, or even Human-Serum Albumin).

3.2. Decay of ^{188}Re and its Energy Spectra

Radioisotope ^{188}Re decays with the half-life of 17 hours emitting β particles (electrons) with a maximum energy of 2.2MeV and also several gamma photons (see Table **1**) [54, 55]. The strongest group of photons, with the energy of 155keV (15%), is well suited for imaging with SPECT camera. Further advantages of ^{188}Re are its low cost and the fact that it can be obtained from a generator [42, 56]. Finally, as from the chemical perspective, ^{188}Re shows close resemblance to ^{99m}Tc, the same molecule can potentially be labelled with ^{99m}Tc for diagnosis and with ^{188}Re for TRT, making this pair ideal for theranostic applications. If the same molecule can be labeled with ^{99m}Tc and with ^{188}Re, imaging of ^{99m}Tc labeled compound can provide clinicians with diagnostic information. Additionally, dosimetry estimates performed for ^{99m}Tc can be used to predict doses which will be delivered after injection of the same compound labeled with^{188}Re.

Unfortunately, in spite of all these advantages, imaging of ^{188}Re is not easy. This is because ^{188}Re electromagnetic emissions, besides the 155keV photons which can be used for imaging, include bremsstrahlung (BRS) photons (generated by interactions of β particles with tissue) and several high-energy gammas. Both, BRS and down-scattered high energy photons create substantial background underneath the 155keV photopeak. Figure **1** show an

example of the simulated spectrum of photons which will be created in water by a ^{188}Re source. In this case a 1cm radius sphere filled with activity was placed in a 20cm diameter water phantom.

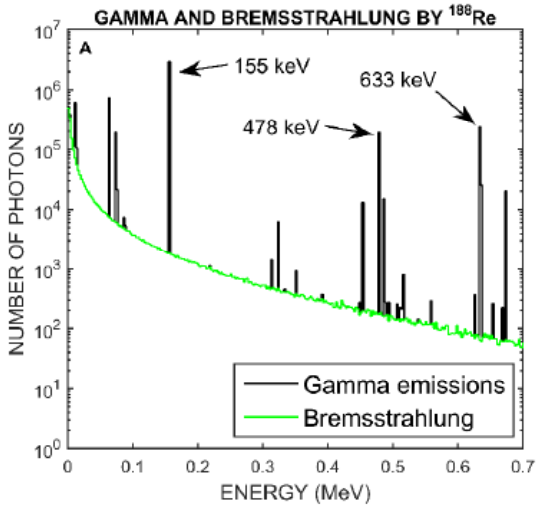

Figure 1: Simulated energy spectrum of the electromagnetic emissions accompanying ^{188}Re decay. The spectrum represents photons created by a 1cm radius sphere filled with activity placed in a 20cm diameter water phantom.

3.3. Optimizing ^{188}Re Acquisitions

The shape of the energy spectrum in Figure **1** becomes substantially modified when photons are recorded by the camera with a collimator. Figure **2** shows the change to the spectrum which was presented in Figure **1** caused by acquisition with the camera equipped with low energy (LE), medium energy (ME) and high energy (HE) collimators. Both, the detector (3/8" NaI crystal) and the collimator efficiencies were modeled in our simulations [57].

Table **2** shows the relative contributions of primary, scattered (self-scattered and down-scattered) and BRS photons recorded in the 20% energy window centered on the 155keV photopeak. The analysis of the data in Figure **2** and Table **2** clearly indicates that, in spite of the fact that ^{188}Re imaging is based on the low energy photons, the HE collimator should be used in patient imaging studies as it will create the best imaging conditions and will minimize contribution of different contaminants to the photopeak window.

The same data also indicate that, although correction for BRS may not be necessary, scatter correction is essential, as even for the HE collimator, more than 60% of photons recorded in the photopeak window are not primary photons. The scatter correction should be applied to the data irrespectively of the acquisition method, planar or tomographic. Although the TEW scatter correction technique is only an approximation, it should be recommended for imaging of ^{188}Re because of its ability to remove background from BRS and down-scatter.

Table 2: Relative Contributions of Primary, Self-Scatter, Down-Scatter and Bremsstrahlung Photons to the 20% Energy Window Centered on 155keV Photopeak of ^{188}Re. All Quantities are Expressed as the Percentage of the Total Counts in this Window

	Low-energy (LE) collimator	Medium-energy (ME) collimator	High-energy (HE) collimator
Primary	5.2	23.5	36.1
Self-scatter	2.8	13.5	20.7
Down-scatter	88.3	60.5	40.9
Bremsstrahlung	3.7	2.5	2.3

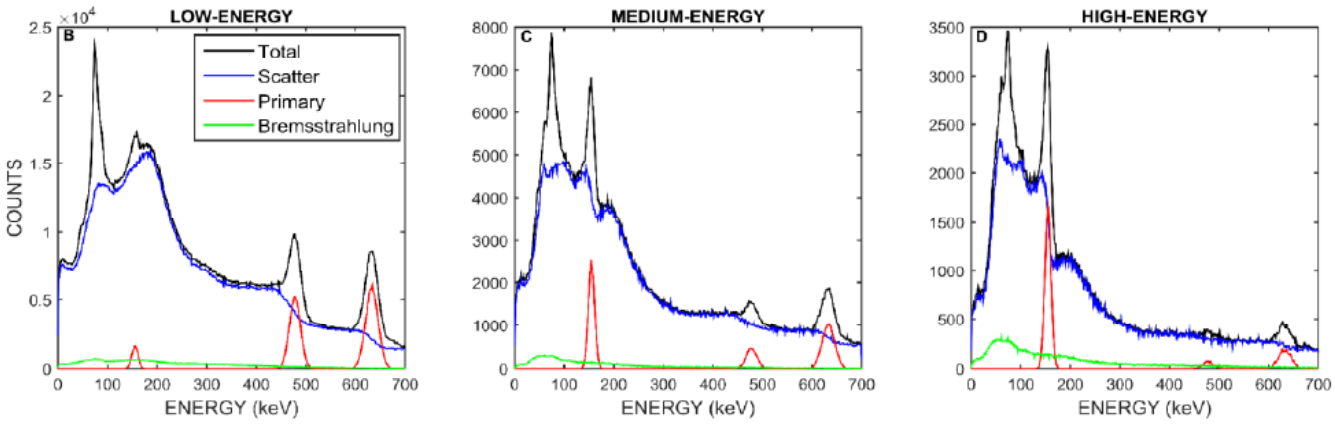

Figure 2: Simulated energy spectra of the ^{188}Re electromagnetic emissions as would be measured by a gamma-camera equipped with low-energy, medium-energy and high-energy collimators.

3.4. Quantification of ^{188}Re Activity in Phantoms

As mentioned above, planar images cannot be properly quantified. However, when using tomographic acquisitions, an accurate quantification is possible when iterative reconstruction with a whole set of corrections is used. In particular, for ^{188}Re, in spite of challenging conditions for data acquisition (Table **2**), the errors in determination of the total activity in the phantom remained below 10% [58]. This accuracy has been achieved with CT-based attenuation, TEW, CDR and DT corrections. Figure **3** analyzes the relative importance of these corrections using an example of our phantom study. In this case, seven hot inserts (activity concentration was 490 kBq/mL for five spheres and 290 kBq/mL for two bottles) were placed in a thorax phantom (with cold lungs and spine inserts) filled with the activity concentration of 70 kBq/mL (source-to-background ratio = 7). The image of the true activity distribution was created from the CT image filled with true activities, as measured in an Atomlab100-plus dose calibrator (Biodex Medical Systems, USA).

Visual analysis of images presented in Figure **3B** and **3C** clearly shows increased activity levels after attenuation correction is applied. Including scatter correction in the reconstruction (Figure **3D**) improves contrast and removes counts from the cold regions. Finally, performing resolution recovery correction (CDR) further improves contrast and decreases partial volume effect. However, for small objects with sharp boundaries, a well-known Gibbs artefact (slight overestimation of activity in the center) can be observed. This artefact is very unlikely to appear in patient studies.

Table **3** analyzes the recovery of activity in three of the seven hot inserts placed inside the phantom. The objects selected in this example are a large 196 mL

Table 3: Recovery of ^{188}Re Activity (MBq) in Two Spheres (S1 and S2) and a Bottle (B1) Placed Inside the Thorax Phantom FIlled with Radioactive Water. The Images were Acquired with HE Collimator and Reconstructed with no Corrections, AC Only, AC+SC and AC+SC+CDR. The Objects were Segmented using their CT Images

Object (Volume)	True Activity (MBq)	Applied Corrections			
		None	AC	AC+SC	AC+SC+CDR
S1 (8 mL)	3.9	0.4	1.8	1.4	2.2
S2 (20 mL)	9.6	1.3	6.2	4.9	6.7
B1(196 mL)	56.3	11.4	59.1	44.5	49.0
Entire phantom	491	206.7	845.3	487.3	495.7

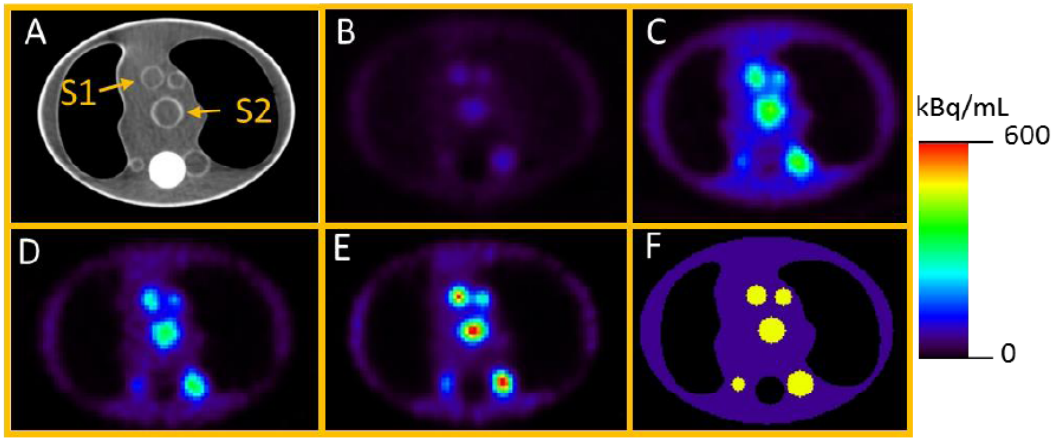

Figure 3: Transaxial slices of the SPECT/CT study of a thorax phantom filled with ^{188}Re. The phantom contains seven hot inserts (five are visible in this slice) and cold lungs and spine. The sequence of images shows the effects of corrections on the quality and quantitative accuracy of the reconstructed images. The geometry of the phantom is depicted in the CT image (**A**), then the sequence of SPECT images follows: with no correction (**B**), attenuation correction (**C**), attenuation and TEW scatter (**D**), attenuation, TEW scatter and CDR corrections (**E**), true activity distribution (**F**). The total activity in the phantom was 491 MBq, resulting negligible camera dead-time. All images are displayed using the same maximum of the colour-scale.

bottle, (object B1, not shown on Figure **3**) and two spheres: one medium size 20mL (object S2) and one small 8mL (object S1). As expected, when no corrections were applied during reconstruction (Figure **3B**), large underestimation of activity in the objects was observed. The use of attenuation correction without compensation for scatter (Figure **3C**) improved the overall quantification accuracy in small objects and, for the example shown here, it yielded better activity recovery than when the image was corrected for scatter (Figure **3D**). However, this apparent good recovery was caused by a substantial over-estimation of activity due to the large amount of scatter photons in the photopeak window that were not removed from the image. The application of CDR improved the recovery of activity for all objects within the phantom; its effect was most noticeable in small objects (sphere S1 and S2 on Figure **3**).

The limited accuracy of activity recovery in small objects is due to the partial volume effect which causes substantial spill-out. This effect is particularly pronounced in our data, where CT-based segmentation was used. On the other hand, the accuracy of quantitative correction can be demonstrated when total counts in the entire phantom are analyzed. In this case, the recovery of the total activity in the phantom compared with its true activity showed less than 2% difference.

3.5. Patient Study

Figure **4** shows a similar comparison of the performance of different quantitative corrections as was presented in Figure **3**, this time applied to the patient study. Obviously, in this case the true activity distribution could not be known. The patient received 1.3GBq of ^{188}Re-HDD-Lipiodol for trans-arterial radioembolization treatment. The scan was performed using a SymbiaT camera (Siemens Medical, Germany) with HE collimator and only negligible camera dead-time was observed. The images illustrate the effects of corrections on the quality and quantitative accuracy of the reconstructed images. The CT image shows the Lipiodol distribution in patient's liver (Figure **4A**), the following images show ^{188}Re activity distribution in the corresponding slice of SPECT images. The images were reconstructed with no corrections (Figure **4B**), with attenuation correction only (Figure **4C**), with attenuation and TEW scatter corrections (Figure **4D**), and with attenuation, TEW scatter and CDR corrections (Figure **4E**). To better illustrate the effects of corrections, all the images are displayed using the same maximum of the colour-scale.

The images presented in Figure **5** illustrate the influence of organ segmentation on dosimetry estimates. Transaxial slices of the liver images of two patients (A and B) having tumours with substantially

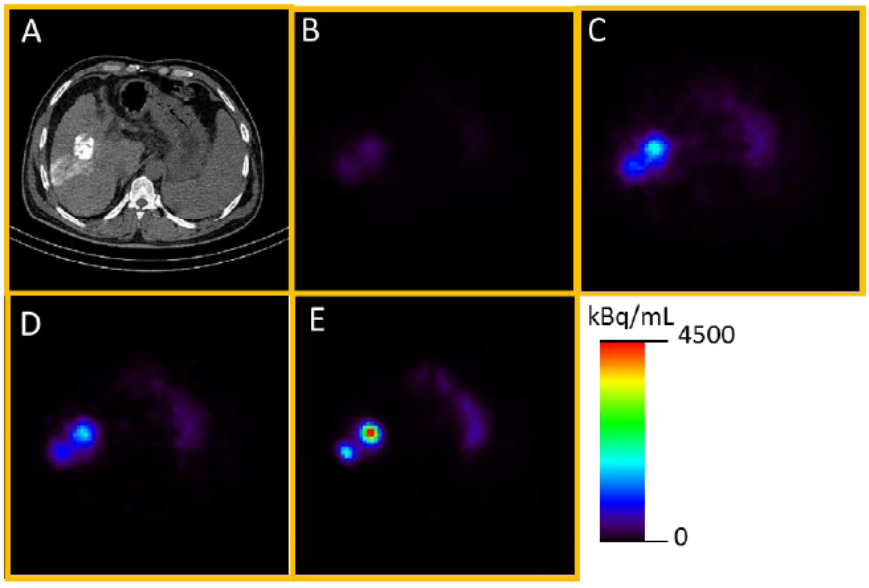

Figure 4: Transaxial slices of the SPECT/CT study of a patient (Patient A) that received trans-arterial radioembolization treatment with ^{188}Re-HDD-Lipiodol. The sequence of images shows the effects of corrections on the quality and quantitative accuracy of the reconstructed images. The patient anatomy showing the Lipiodol distribution in liver is depicted in the CT image (**A**), then the sequence of SPECT images follows: with no correction (**B**), attenuation correction only (**C**), attenuation and TEW scatter (**D**), attenuation, TEW scatter and CDR corrections (**E**). The projection data was acquired with the HE collimator. All images are displayed using the same maximum of the colour-scale.

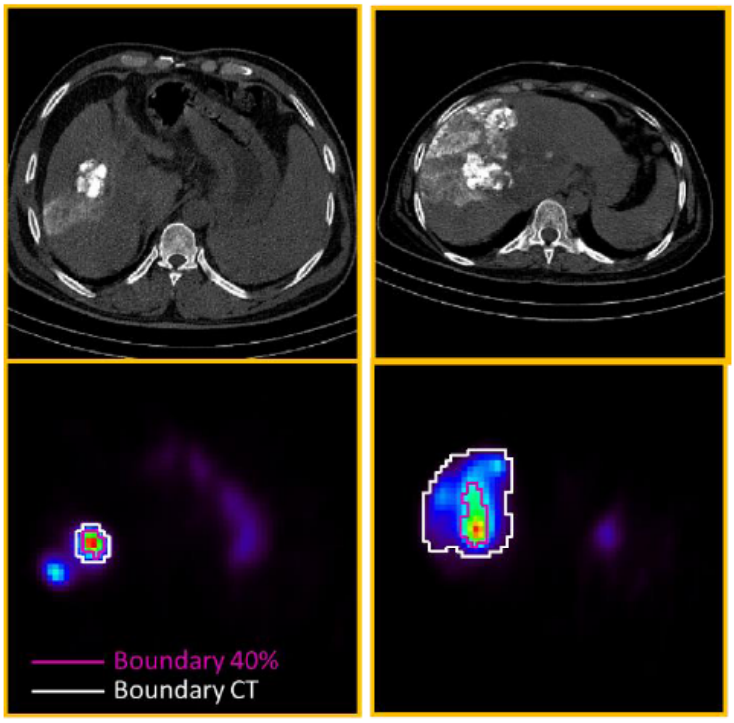

Figure 5: Transaxial slices of SPECT/CT study of two patients (Patient **A** and Patient **B**) that received trans-arterial radioembolization treatment with ^{188}Re-HDD-Lipiodol. The SPECT images were reconstructed with attenuation, TEW scatter and CDR corrections. The boundaries of the tumors, shown on SPECT images, were determined by applying a fixed threshold that recovered the true tumor volumes obtained from contrast-CT images ('Boundary CT') and by applying a fixed 40% threshold.

different sizes are displayed. The volume of both tumours were determined from pre-treatment contrast CT images and were equal to 22cc and 400cc in Patient A and Patient B, respectively. The tumors were segmented by applying a threshold that recovered the true tumor volumes (referred in Figure **5** as 'Boundary CT') and by applying a fixed 40% threshold ('Boundary 40%'). For both patients, the 40% threshold segmentation yielded smaller (patient A) and substantially smaller (patient B) tumour volumes than those obtained from contrast-CT images (considered to be true volumes). This difference was particularly large for Patient 2, where the activity distribution in the tumor was nonuniform, as in this case threshold value was determined based on a very small area with high activity.

At the next step, the effects of using these two different segmentation methods on the absorbed dose estimation were evaluated. The dose values obtained using tumour activities estimated with the CT-based method were always lower than those from the 40% threshold segmentation. The difference was only 50% for Patient A, but reached 140% level for Patient B. This analysis clearly indicated crucial importance of accurate segmentation method.

Additionally, the effects of timing the imaging scans used to create TACs on the patient dose were estimated. The patient used in this example (Patient B) was scanned (whole-body planar and SPECT/CT) at 3h, 24h and 48h after the administration of ^{188}Re-HDD-Lipiodol. The dosimetry calculations presented in Table **4** were performed using TACs derived from the data acquired at three time-point (method A), using only two out of these three time-points (methods B and C) and using one time point with the physical half-life of ^{188}Re (method D). The dose estimated using method A with three data-points was 20% higher than that calculated based on only two scans (methods B and C). The effective half-life of ^{188}Re-HDD-Lipiodol in tumor derived from the three time-points was 12.8h, while two data point yielded 10.3h and 16.2h. However, the dose estimated using physical half-life was substantially higher that that obtained based on the imaging data.

In summary, this analysis illustrates the impact of the method used for organ segmentation and the importance of the appropriate imaging protocol when estimating dose in radionuclide therapies. Although in this study we used only a few limited examples of phantom and patient data, our on-going analysis of the

Table 4: Comparison the Mean Radiation doses Absorbed by Liver Tumour of a Patient Who Received ^{188}Re-HDD-Lipiodol Radioembolization (Patient B from Figure 5). The Estimates Were Calculated Using Time-Integrated Activities Based on Tacs Determined from: The Sequence of three Scans (A), Only Two Scans (B) and (C), and One Scan Assuming Radioisotope Clearance With Physical Half-Life Only (D). The Injected Activity was 1.7GBq and the Images were Reconstructed With All Corrections (*i.e.*, AC+SC+CDR)

	TAC Determination Method			
	A	**B**	**C**	**D**
Time schedule	{3h, 24h, 48h}	{3h, 24h}	{24h, 48h}	{3h}
T_{eff}[h]	12.8	10.3	16.2	T_{phys} = 17
Tumor Dose [Gy] (CT segmentation)	11.26	9.44	9.37	14.36

larger patient populations confirms the observed trends.

CONCLUSIONS

Radionuclide therapies are gaining recognition for their potential to deliver targeted treatment directly to tumour sites using molecular nuclear medicine approaches. However, current treatments mostly use 'one-size-fits-all' radiopharmaceutical administration, while the increasing body of evidence suggests that plans based on personalized dosimetry calculation do improve treatment outcomes, at the same time minimizing toxicity. Recent studies have shown that accurate image-based dosimetry is not only possible, but also highly recommended by the MIRD community [9]. However, advanced methods, based on tomographic quantitative imaging (SPECT and PET) and taking into account the particularities of the decay and emissions of the therapeutic radioisotope in question must be employed. This attitude motivates the creation of specialized dosimetry guidelines, such as the recently published MIRD pamphlets for ^{131}I [59] and ^{177}Lu [60].

The material presented in this paper follows this philosophy. It outlines the procedures required for performing accurate personalized dose calculations based on quantitative SPECT studies and discusses their application for ^{188}Re therapies.

ACKNOWLEDGEMENTS

This research was supported by a Collaborative Health Research Projects grant from the Natural Sciences and Engineering Research Council (NSERC) in Canada and the Canadian Institutes of Health Research (CIHR) (Grant No. CHRP 413975-12). The authors would like to thank Dr. Ajit Shinto and Jephy Joseph from the Nuclear Medicine Department at Kovai Medical Center and Hospital (Coimbatore, India) for providing us with the patient images used in the study; and the staff of the Nuclear Medicine Department at the Vancouver General Hospital for their patience and help in our experiments.

REFERENCES

[1] Cameron AT. Radium and radioactivity. Society for promoting Christian knowledge 1912.

[2] MacKee GM, X-rays and radium in the treatment of diseases of the skin, Lea & Febiger 1921.

[3] Ersahin D, Doddamane I, Cheng D, Targeted Radionuclide Therapy, Cancers 2011; 3: 3838-3855 https://doi.org/10.3390/cancers3043838

[4] Graham MM, Weber WA, Evaluation of the Efficacy of Targeted Imaging Agents, J Nucl Med 2016; 57:653-659 https://doi.org/10.2967/jnumed.115.169235

[5] Zukotynski K, Jadvar H, Capala J, Fahey F. Targeted Radionuclide Therapy: Practical Applications and Future Prospects, Biomarkers in Cancer 2016; 8: 35-38. https://doi.org/10.4137/BIC.S31804

[6] Grimes J, Celler A, Birkenfeld B, Shcherbinin S, Listewnik MH, Piwowarska-Bilska H *et al*., Patient-Specific Radiation Dosimetry of 99mTc-HYNIC-Tyr3-Octreotide in Neuroendocrine Tumors. J Nucl Med 2011; 52:1474-81. https://doi.org/10.2967/jnumed.111.088203

[7] Beauregard JM, Hofman MS, Kong G, Hicks RJ, The tumour sink effect on the biodistribution of 68Ga-DOTA-octreotate: implications for peptide receptor radionuclide therapy, Eur J Nucl Med Mol Imaging 2012; 39: 50-56 https://doi.org/10.1007/s00259-011-1937-3

[8] Svensson J, Berg G, Wängberg B, Larsson M, Forssell-Aronsson E, Bernhardt P. Renal function affects absorbed dose to the kidneys and haematological toxicity during 177Lu-DOTATATE treatment, Eur J Nucl Med Mol Imaging 2015; 42:947-955 https://doi.org/10.1007/s00259-015-3001-1

[9] Dewaraja YK, Frey EC, Sgouros G, Brill AB, Roberson P, Zanzonico PB *et al*. MIRD Pamphlet No. 23: Quantitative SPECT for Patient-Specific 3-Dimensional Dosimetry in Internal Radionuclide Therapy, J Nucl Med 2012; 53: 1-16. https://doi.org/10.2967/jnumed.111.100123

[10] Lambert B, de Klerk JMH. Clinical applications of 188Re-labelled radiopharmaceuticals for radionuclide therapy, Nucl Med Comm 2006; 27: 223-229. https://doi.org/10.1097/00006231-200603000-00004

[11] Sundram F, Chau TCM, Onkhuudai P, Bernal P, Padhy AK. Preliminary results of transarterial rhenium-188 HDD lipiodol in the treatment of inoperable primary hepatocellular carcinoma, Eur J Nucl Med Mol Imaging 2004; 31: 250-257. https://doi.org/10.1007/s00259-003-1363-2

[12] Nowicki ML, Cwikła JB, Sankowski A, Shcherbinin S, Grimes J, Celler A *et al*., Initial radiological and clinical efficacy of radioembolisation using 188Re-Human Serum Albumin (HAS) spheres in patients with progressive, unresectable primary or secondary liver cancers. A phase II study, Medical Science Monitor 2014; 20: 1353-1362. https://doi.org/10.12659/MSM.890480

[13] Strigari L, Konijnenberg M, Chiesa C, Bardies M, Du Y, Sjögreen Gleisner K *et al*., The evidence base for the use of internal dosimetry in the clinical practice of molecular radiotherapy, Eur J Nucl Med Mol Imaging 2014; 41: 1976-1988. https://doi.org/10.1007/s00259-014-2824-5

[14] Garkavij M, Nickel M, Sjogreen-Gleisner K, Ljungberg M, Ohlsson T, Wingardh K *et al*., 177Lu-[DOTA0, Tyr3] octreotate therapy in patients with disseminated neuroendocrine tumors: Analysis of dosimetry with impact on future therapeutic strategy, Cancer 2010; 116(4 Suppl): 1084-92 https://doi.org/10.1002/cncr.24796

[15] Sandström M, Garske U, Granberg D, Sundin A, Lundqvist H. Individualized dosimetry in patients undergoing therapy with 177Lu-DOTA-D-Phe (1)-Tyr (3)-octreotate. Eur J Nucl Med Mol Imaging 2010; 37: 212-25. https://doi.org/10.1007/s00259-009-1216-8

[16] Bolch WE, Eckerman KF, Sgouros G, Thomas SR. MIRD Pamphlet No. 21: A Generalized Schema for Radiopharmaceutical Dosimetry-Standardization of Nomenclature, J Nucl Med 2009; 50: 477-484 https://doi.org/10.2967/jnumed.108.056036

[17] Stabin MG, Sparks RB, Crowe E. OLINDA/EXM: the second-generation personal computer software for internal dose assessment in nuclear medicine. J Nucl Med 2005; 46: 1023-1027

[18] Radar Webpage (2017), http://www.doseinfo-radar.com/RADAR-INT-NM.html

[19] Divoli A, Chiavassa S, Ferrer L, Barbet J, Flux GD, Bardies M. Effect of Patient Morphology on Dosimetric Calculations for Internal Irradiation as Assessed by Comparisons of Monte Carlo Versus Conventional Methodologies, J Nucl Med 2009; 50: 316-323 https://doi.org/10.2967/jnumed.108.056705

[20] Stabin MG, Xu XG, Emmons MA, Segars WP, Shi C, Fernald MJ. RADAR Reference Adult, Pediatric, and Pregnant Female Phantom Series for Internal and External Dosimetry, J Nucl Med 2012; 53: 1-7 https://doi.org/10.2967/jnumed.112.106138

[21] Amato E, Italiano A, Baldari S. Monte Carlo study of voxel S factor dependence on tissue density and atomic composition, Nuclear Instruments and Methods in Physics Research 2013; A729: 870-876 https://doi.org/10.1016/j.nima.2013.08.059

[22] Lanconelli N, Pacilio M, Lo Meo S, Botta F, Di Dia A, Torres Aroche AL *et al*., A free database of radionuclide voxel S values for the dosimetry of nonuniformactivity distributions Phys Med Biol 2012; 57: 517-33 https://doi.org/10.1088/0031-9155/57/2/517

[23] Sarrut D, Bardiès M, Boussion N, Freud N, Jan S, Létang JM *et al*., A review of the use and potential of the GATE Monte Carlo simulation code forradiation therapy and dosimetry applications, Medical Physics 2014; 41(6): 064301-14 https://doi.org/10.1118/1.4871617

[24] Villoing D, Sara Marcatili S, Garcia MP, Bardiès M. Internal dosimetry with the Monte Carlocode GATE: validation using the ICRP/ICRU female reference computational model, Phys Med Biol 2017; 62: 1885-1904 https://doi.org/10.1088/1361-6560/62/5/1885

[25] He B, Wahl RL, Du Y, Sgouros G, Jacene H, Flinn I *et al*., Comparison of Residence Time Estimation Methods for Radioimmunotherapy Dosimetry and Treatment Planning-Monte Carlo Simulation Studies. IEEE Trans Med Imaging 2008; 27: 521-30 https://doi.org/10.1109/TMI.2007.908131

[26] Assie K, Dieudonne A, Gardin I, Buvat I, Tilly H, Vera P. Comparison between 2D and 3D dosimetry protocols in 90Y-ibritumomab tiuxetan radioimmunotherapy of patients with non-Hodgkin's lymphoma. Cancer Biother Radiopharm 2008; 23: 53-64 https://doi.org/10.1089/cbr.2007.372

[27] Shepp LA, Vardi Y. Maximum likelihood reconstruction for emission tomography. IEEE Trans Med Imaging 1982; 1: 113-122 https://doi.org/10.1109/TMI.1982.4307558

[28] Hudson HM, Larkin RS. Accelerated image reconstruction using ordered subsets of projection data, IEEE Trans Med Imaging 1994; 13: 601-609 https://doi.org/10.1109/42.363108

[29] Hutton BF, Buvat I, Beekman FJ. Review and current status of SPECT scatter correction, Phys Med Biol 2011; 56: R85-R112 https://doi.org/10.1088/0031-9155/56/14/R01

[30] Ogawa K, Harata Y, Ichihara T, Kubo A, Hashimoto S. A Practical Method for Position-Dependent Compton-Scatter Correction in Single Photon Emission CT, IEEE Tran Med Imag 1991; 10: 408-412 https://doi.org/10.1109/42.97591

[31] Beauregard JM, Hofman MS, Pereira JM, Eu P, Hicks RJ. Quantitative Lu-177 SPECT (QSPECT) imaging using a commercially available SPECT/CT system, Cancer Imaging 2011; 11: 56-66 https://doi.org/10.1102/1470-7330.2011.0012

[32] Celler A, Uribe CF, Esquinas PL, Gonzalez M. Dead-time corrections for quantitation of Lu-177 SPECT/CT radionuclide therapy studies, Annual Congress of European Association of Nuclear Medicine 2014.

[33] Celler A, Piwowarska-Bilska H, Shcherbinin S, Uribe CF, Mikolajczak R, Birkenfeld B. Evaluation of dead-time corrections for post-radionuclide therapy Lu-177 quantitative imaging with low-energy high-resolution collimators. Nucl Med Commun 2014; 35: 73-87 https://doi.org/10.1097/MNM.0000000000000011

[34] Shcherbinin S, Grimes J, Bator A, Cwikla JB, Celler A. Three-dimensional personalized dosimetry for Re-188 liver selective internal radiation therapy based on quantitative post-treatment SPECT studies. Phys Med Biol 2014; 59: 119-34 https://doi.org/10.1088/0031-9155/59/1/119

[35] Uribe CF, Esquinas PL, Tanguay J, Gonzalez M, Gaudin E, Beauregard JM, *et al*., Accuracy of Lu-177 activity quantification in SPECT imaging: a phantom study. Eur J Nucl Med Mol Imaging Phys 2017; 4: 2-20

[36] Erdi YE, Wessels BW, Loew MH, Erdi K. Threshold estimation in single photon emission computed tomography and planar imaging for clinical radioimmunotherapy, Cancer Res 1995; 55: 5823s-5826s

[37] Biehl KJ, Kong F, Dehdashti F, Jin J, Mutic S, El Naqa I, *et al*., 18F-FDG PET Definition of Gross Tumor Volume for Radiotherapy of Non-Small Cell Lung Cancer: Is a Single Standardized Uptake Value Threshold Approach Appropriate?. J Nucl Med 2006; 47: 1808-12

[38] Shepherd T, Teräs M, Beichel RR, Boellaard R, Bruynooghe M, Dicken V, *et al*., Comparative study with new accuracy metrics for target volume contouring in PET image guided radiation therapy, IEEE Tran Med Imag 2012; 31: 2006-2014 https://doi.org/10.1109/TMI.2012.2202322

[39] Pacilio M, Basile C, Shcherbinin S, Caselli F, Ventroni G, Aragno D *et al*., An innovative iterative thresholding algorithm for tumour segmentation and volumetric quantification on SPECT images: Monte Carlo-based methodology and validation, Med Phys 2011; 38(6): 3050-61 https://doi.org/10.1118/1.3590359

[40] Grimes J, Celler A, Shcherbinin S, Piwowarska-Bilska H, Birkenfeld B. The accuracy and reproducibility of SPECT target volumes and activities estimated using an iterative adaptive thresholding technique, Nuclear Medicine Communications 2012; 33: 1254-126 https://doi.org/10.1097/MNM.0b013e3283598395

[41] Hatt H, Lee J, Schmidtlein CR, El Naqa I, Caldwell C, De Bernardi E *et al*., Classification and evaluation strategies of auto-segmentationapproaches for PET: Report of AAPM Task Group No. 211, Med Phys 2017 (Ahead of print).

[42] Argyrou M, Valassi A, Andreou M, Lyra M. Rhenium-188 Production in Hospitals, by W-188/Re-188 Generator, for Easy Use in Radionuclide Therapy, International Journal of Molecular Imaging 2013, Article ID 290750 https://doi.org/10.1155/2013/290750

[43] Liepe K, Kropp J, Runge R, Kotzerke J. Therapeutic efficiency of rhenium-188-HEDP in human prostate cancer skeletal metastases, Br J Cancer 2003; 89: 625-629 https://doi.org/10.1038/sj.bjc.6601158

[44] Wang SJ, Lin WY, Hsieh BT, Shen LH, Tsai ZT, Tinge G, FF Knapp Jr. FF. Rhenium-188 sulphur colloid as a radiation synovectomy agent, Eur J Nucl Med 1995; 22: 505-507 https://doi.org/10.1007/BF00817272

[45] Shamim SA, Kumar R, Halanaik D, Kumar A, Shandal V, Shukla J *et al*., Role of rhenium-188 in colloid radiosynovectomy in patients with inflammatory knee joint conditions refractory to conventional therapy, Nuclear Medicine Communications 2010; 31: 814-820 https://doi.org/10.1097/MNM.0b013e32833d6869

[46] Werner M, Scheinert D, Henn M, Scheinert S, Bräunlinch S, Bausback Y *et al*., Endovascular brachytherapy using liquid beta-emitting Rhenium-188 for the treatment of long-segment femoropopliteal in-stent stenosis, J Endovasc Ther 2012; 19: 467-475 https://doi.org/10.1583/12-3832R.1

[47] Kotzerke J, Glatting G, Seitz U, Rentschler M, Neumaier B, Bunjes D, *et al*., Radioimmunotherapy for the intensification of conditioning before stem cell transplantation: differences in dosimetry and biokinetics of 188Re- and 99mTc-labeled anti-NCA-95 MAbs, J Nucl Med 2000; 41: 531-537

[48] Juweid M, Sharkey RM, Swayne LC, Griffiths GL, Dunn R, Goldenberg DM. Pharmacokinetics, dosimetry and toxicity of Rhenium-188-labelled anti-carcinoembryonic antigen monoclonal antibody, MN-14, in gastrointestinal cancer, J Nucl Med 1998; 39: 34-42

[49] Edelman MJ, Clamon G, Kahn D, Magram M, J Lister-James, BR Line. Targeted radiopharmaceutical therapy for advanced lung cancer: phase I trial of rhenium Re188 P2045, a somatostatin analog, J Thorac Oncol 2009; 4: 1550-1554 https://doi.org/10.1097/JTO.0b013e3181bf1070

[50] Bernal P, Raoul JL, Vidmar G, Sereegotov E, Sundram F X, Kumar A *et al*., Intra-Arterial Rhenium-188 Lipiodol in the Treatment of Inoperable Hepatocellular Carcinoma: Results of an IAEA-Sponsored Multination Study Int J Radiat Oncol Biol Phys 2007; 69: 1448-55 https://doi.org/10.1016/j.ijrobp.2007.05.009

[51] Liepe K, Brogsitter C, Leonhard J, Wunderlich G, Hliscs R, Pinkert J *et al*., Feasibility of high activity Rhenium-188-microsphere in hepatic radioembolization, Jpn J Clin Oncol 2007; 37(12): 942-950 https://doi.org/10.1093/jjco/hym137

[52] Zanzonico PB, Divgi C. Patient-specific radiation dosimetry for radionuclide therapy of liver tumors with intrahepatic artery Rhenium-188 Lipiodol, Seminar in Nuclear Medicine 2008; 38: 30-39 https://doi.org/10.1053/j.semnuclmed.2007.10.005

[53] Madsen MT, Park CH, Thakur ML. Dosimetry of idodine-131 ethiodol in the treatment of hepatoma, J Nucl Med 1988; 29: 1038-44

[54] Singh B. Nuclear Data Sheets for A = 188 Nucl. Data Sheets 2002; 95: 387-541 https://doi.org/10.1006/ndsh.2002.0005

[55] NNDC – National Nuclear Data Center (2017), Brookhaven National Laboratory webpage http://www.nndc.bnl.gov/

[56] Pillai MRA, Dash A, Knapp Jr FF. Rhenium-188: Availability from the 188W/188Re Generator and Status of Current Applications, Radiopharmaceuticals 2012; 5: 228-243 https://doi.org/10.2174/1874471011205030228

[57] Uribe CF, Esquinas PL, Gonzalez, M, Celler A. Characteristics of Bremsstrahlung emissions of 177Lu, 188Re and 90Y for SPECT/CT quantification in radionuclide therapy, Phys Med 2016; 32: 691-700 https://doi.org/10.1016/j.ejmp.2016.04.014

[58] Esquinas PL, Uribe CF, Tanguay J, Gonzalez M, Rodríguez-Rodríguez C, Häfeli UO *et al*., Optimizing 188Re SPECT/CT: Quantitative Imaging for Image-based Dosimetry, Eur J Nucl Med Mol Imaging 2016; 43 (Suppl 1)

[59] Dewaraja YK, Ljungberg M, Green A, Zanzonico PB, Frey EC, SNMMI MIRD Committee *et al*., MIRD Pamphlet No. 24: Guidelines for Quantitative 131I SPECT in Dosimetry Applications, J Nucl Med 2013; 54: 2182-2188 https://doi.org/10.2967/jnumed.113.122390

[60] Ljungberg M, Celler A, Konijnenberg MW, Eckerman KF, Dewaraja YK, Sjögreen-Gleisner K. MIRD Pamphlet No. 26: Joint EANM/MIRD Guidelines for Quantitative 177 Lu SPECT Applied for Dosimetry of Radiopharmaceutical Therapy, J Nucl Med 2016; 57:151-162 https://doi.org/10.2967/jnumed.115.159012

Received on 23-03-2017 Accepted on 12-04-2017 Published on 31-07-2017

http://dx.doi.org/10.15379/2408-9788.2017.05